Vol 17 No 6, June 2008
1674-1056/2008/17(06)/2281-07

Chinese Physics B

© 2008 Chin. Phys. Soc.
and IOP Publishing Ltd

Magnetic domain structures of precipitation-hardened SmCo 2:17-type sintered magnets: Heat treatment effect*

Li Xiu-Mei(李岫梅)[a)†], Fang Yi-Kun(方以坤)[a)], Guo Zhao-Hui(郭朝晖)[a)], Liu Tao(刘 涛)[a)], Guo Yong-Quan(郭永权)[a)], Li Wei(李 卫)[a)], and Han Bao-Shan(韩宝善)[b)]

[a)] *Division of Functional Materials Research, Central Iron & Steel Research Institute, Beijing* 100081, *China*
[b)] *State Key Laboratory of Magnetism, Institute of Physics and the Center for Condensed Matter Physics, Chinese Academy of Sciences, Beijing* 100190, *China*

(Received 17 November 2007; revised manuscript received 13 December 2007)

The typical magnetic domains of $Sm(Co_{bal}Fe_{0.25}Cu_{0.07}Zr_{0.02})_{7.4}$ magnets quenched through various heat-treatment steps have been revealed by using magnetic force microscopy (MFM). For the specimens in which the nominal *c*-axis is perpendicular to the imaging plane, the domain configurations change from plate-like for the as-sintered magnet to corrugation and spike-like for the homogenized one, and then to a coarse and finally to a finer domain structure when isothermally aged at 830°C and then annealed at 400°C. However, only plate-like domains can be detected on the surfaces with the nominal *c*-axis parallel to the imaging plane. The finer domain (so-called interaction domain) is a characteristic magnetic domain pattern of the Sm–Co 2:17-type magnets with high coercivities. Domain walls in a zigzag shape are revealed by means of MFM in final bulk Sm–Co 2:17-type sintered magnets.

Keywords: Sm–Co permanent magnets, magnetic domains, heat-treatment, magnetic force microscopy

PACC: 7560G, 7560C

1. Introduction

The $Sm(Co,Fe,Cu,Zr)_z$ ($z = 7.0 - 8.5$) permanent magnets have been reported to be able to operate at temperatures above 500°C, and they are possessed of high coercivity and high Curie temperature (about 820°C).[1−3] Very complex production processes, which involve sintering, homogenizing, isothermal aging and slow cooling, result in the formation of a cellular precipitation structure which acts as pinning centres for magnetic domain wall motion.[4] The cellular microstructure has been investigated widely,[5−7] and it consists of the $Sm_2(Co, Fe)_{17}$-cell matrix phase, the $Sm(Co, Cu)_5$-cell boundary phase and the Zr-rich lamella phase. The average size is about 100–200 nm for 2:17 main phase and 10 nm for 1:5 boundary phase.

Although there have been numerous publications on SmCo 2:17-type magnets, only few magnetic domain characterizations on SmCo 2:17-type sintered magnets have been investigated.[8−10] Zhang *et al*[8] studied the domain structure of the precipitation hardened 2:17-type Sm–Co magnets using Lorentz microscopy, revealing the pinning effect of domain walls. Xia *et al*[9] studied the magnetic microstructures of Sm–Co magnets with Sm volatilization at a relatively high temperature, indicating that the Sm volatilization could be suppressed by Ta plating layer of about 20 nm in thickness. However, these studies focused on Sm–Co magnets in a high coercivity state. Recently, Gutfleisch *et al*[10] have reported the domain of SmCo 2:17-type magnets in the course of slowing cooling process, and pointed out that the domain of final magnets is a kind of coupling interaction one. Nevertheless, the reports on magnetic domain configurations of SmCo 2:17-type magnets during the complex heat treatments are limited. Magnetic force microscopy (MFM) with high lateral resolutions of 10–50 nm and easy manipulation is a powerful tool for detecting magnetic domains of permanent magnetic materials.[11,12] In this paper, magnetic domain

*Project supported by the Beijing Municipal Science and Technology Committee Key Project, China (Grant No D0406002000091) and the National Natural Science Foundation of China (Grant No 10374110).
†E-mail: lixiumei55@sohu.com

structures of $Sm(Co,Fe,Cu,Zr)_{7.4}$ sintered magnets are characterized by using MFM after the magnets have been quenched through the four steps of heat treatment, i.e. sintering, solid-solution, isothermal aging and slow cooling, sequentially.

2. Experiment

The SmCo 2:17-type sintered magnets were prepared by powder metallurgy procedures. The alloy ingot with the nominal composition of $Sm(Co_{bal}Fe_{0.25}Cu_{0.07}Zr_{0.02})_{7.4}$ was prepared by vacuum induction melting with an excess 5 wt.% Sm added, and then it underwent a series of processes, such as pulverizing, magnetic powders alignment and subsequent heat treatments, finally the sintered SmCo 2:17-type magnets were obtained. Especially, the heat treatments were sequentially performed through the following four steps: sintering at about 1200°C for 0.5 h, solid-solution treatment at about 1180°C for 5 h, isothermal aging at 830°C for 24 h, and finally slow-cooling at a rate of 0.7°C /min to 400°C, and then soaking for 10 h. In order to reveal the influence of the heat treatment on magnetic domain structures, we gradually quenched specimens from 1200, 1180, 830 and 400°C to room temperature, sequentially. Four groups of corresponding specimens were obtained and labelled as A, B, C and D, respectively. The heat treatment conditions for the specimens A–D are listed in Table 1 in detail.

Table 1. Heat treatment conditions of specimens A–D.

Specimen	Sintering conditions	Solid solution conditions	Homogenizing treatment	Slow cooling conditions
A	1200°C×0.5h	—	—	—
B	1200°C×0.5h	1180°C×5h	—	—
C	1200°C×0.5h	1180°C×5h	830°C×24h	—
D	1200°C×0.5h	1180°C×5h	830°C×24h	0.7K/min, 400°C×10h

The phase constituents of the specimens were analysed by the X-Pert Pro-type x-ray diffractometer using Cu K_α radiation ($\lambda = 0.154\,\mathrm{nm}$). Magnetic properties of the specimens were measured by a VSM and NIM-2000H-type hysteresis loop tracer. Magnetic microstructures of the specimens were detected by Digital Instruments NanoScope IIIa-D3000 magnetic force microscopy (MFM) operating in Tapping/Lift modes, with a Co-Pt coated high coercivity tip (its coercivity $H_c > 80\,\mathrm{kA/m}$) magnetized downwards. The lift-height of the tip is 30nm when scanning. The coercivity of the tip is high enough to ensure that its magnetic moment direction is unperturbed by specimens.[13] For MFM experiments, the observed surfaces were carefully ground and polished using SiC abrasive papers (from 400 down to 1200 grade) and diamond powders (2.5, 1, 0.25 μm in diameter) with a water-free lubricant. In fact, during the procedures stress was inevitably introduced in their surface layers. However, for SmCo-type magnets, we have found that the introduced stress has only a little influence on the intrinsic domain structures, as reported in Refs.[9,13]. Accordingly, in this paper, MFM images are obtained directly on the specimens that have been just polished but not undergone by any further treatments.

3. Results and discussion

Figure 1 shows the XRD powder patterns of the four kinds of SmCo 2:17-type specimens. The specimen (specimen A) only annealed at 1200°C for 0.5 h consists of 1:7H main phase with a $TbCu_7$ structure and a small amount of 1:5 phase with a $CaCu_5$ structure, as shown in Fig.1(a). After the sintered Sm–Co magnets have been solid-solution treated at 1180°C for 5 h, single-phase with 1:7H structure occurs (Fig.1(b)) because of the transformation of 1:5 phase into 1:7H by eutectic reaction. Figures 1(c) and 1(d) show that both specimens C and D consist of 2:17R and 1:5 phases. The two phases form due to the phase separation of the 1:7H after isothermal aging, which is consistent with the fact that the cellular and the lamellar microstructures have formed during the isothermal treatment.[14,15]

Hysteresis loops of specimens A–C and the demagnetization curve of specimen D are shown in Fig.2. It is obvious that specimens A–C show typical soft magnetic behaviours (the intrinsic coercivity ${}_jH_c < 100\,\mathrm{kA/m}$), whereas specimen D exhibits a permanent characterization (${}_jH_c = 2205\,\mathrm{kA/m}$). The behaviour of magnetic properties of specimens A–D accords well

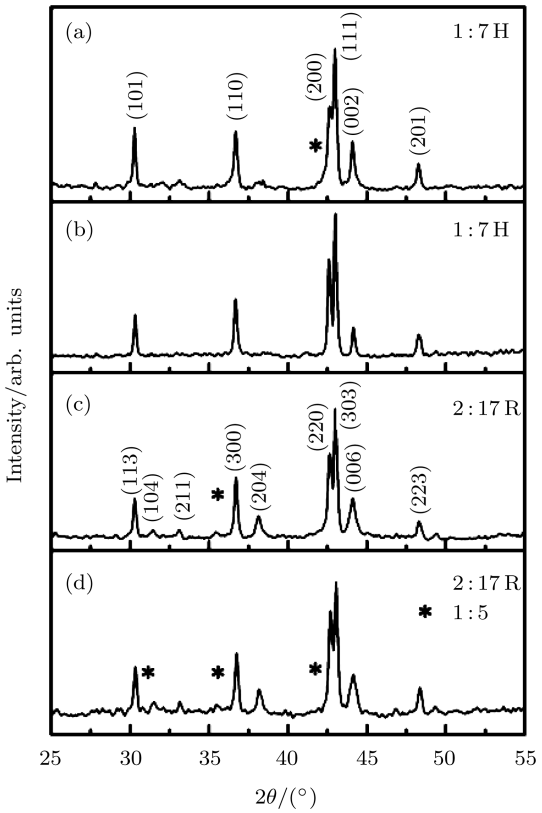


Fig.1. Powder XRD patterns of the four specimens: specimen A (a), specimen B (b), specimen C (c) and specimen D (d).

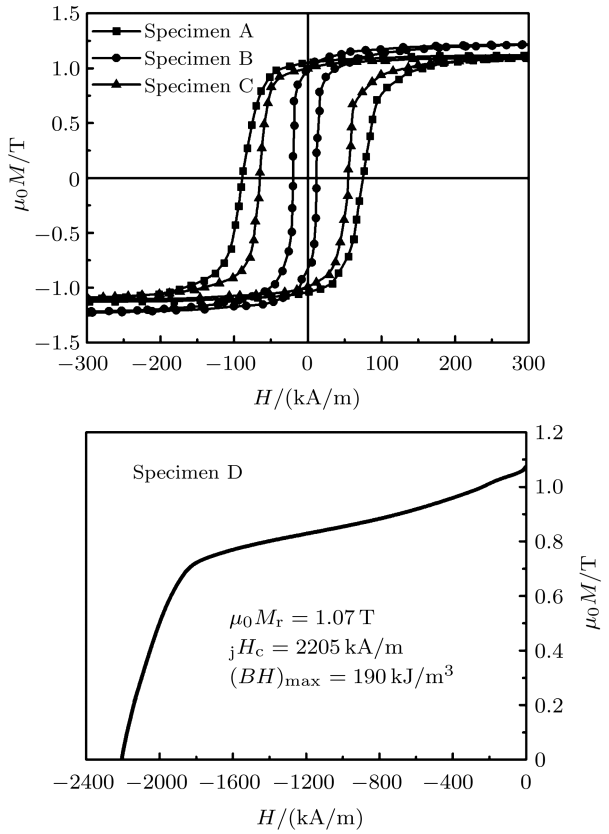


Fig.2. Hysteresis loops of the specimens A–C (upper panel) and demagnetization curve of the specimen D (lower panel).

with that reported by Strnat.[1] It should be pointed out that the intrinsic coercivity of specimen B is only about 13 kA/m, indicating that specimen B is considerably "soft". It can be attributed to its single 1:7H phase (see Fig.1(b)) with a larger average grain size (mentioned below) and less defects in it. Therefore, in the magnetization reversal process of specimen B, the domain walls in the crystals move easily, resulting in lower intrinsic coercivities.

Figure 3 shows typical magnetic domain structures of specimens A–D with the nominal c-axis perpendicular to the imaging plane. On the whole, the magnetic domains of the four specimens differ from each other significantly. For specimen A as shown in Fig.3(a), a stripe domain pattern is present. The average surface domain width, $\langle w\rangle_{\rm s}^{\rm A}$, is measured to be about 0.9 μm by using the Bodenberger and Hubert method,[16,17] and listed in Table 2. However, as seen in Fig.3(b), specimen B takes on typical corrugation and spike domains (i.e. black and white dots). The domain width, $\langle w\rangle_{\rm s}^{\rm B}$, is about 1.5 μm. As is well known, the corrugation and spike domain is a typical domain configuration occurring in the strong magnetic anisotropic crystals with the normal c-axis (easy axis) perpendicular to the imaging plane, for example, $Nd_2Fe_{14}B$ single crystals, according to the two phase branching theory.[17] In order to develop precipitation-hardened SmCo 2:17-type sintered magnet, the isothermal treatment at 830°C for a long time (10–25 h) is needed. As shown in Fig.3(c), the typical magnetic microstructures of specimen C are detected by magnetic tips as coarse domains or wide stripe domains with a domain width ($\langle w\rangle_{\rm s}^{\rm C}$) of about 1.6 μm. It is noted that there is no reverse spike domain in Fig.3(c) though the value of $\langle w\rangle_{\rm s}^{\rm C}$ is similar to that of $\langle w\rangle_{\rm s}^{\rm B}$. This is ascribed to the formation of cellular structure after isothermal treatment at 830°C as mentioned above. Figure 3(d) shows the fine domain structures of specimen D with a high coercivity ($_{\rm j}H_{\rm c}$) of 2205 kA/m and a domain width ($\langle w\rangle_{\rm s}^{\rm D}$) of about 0.5 μm. The similar fine domains have recently been revealed in an optimally processed bulk SmCo

Table 2. Average surface width $\langle w\rangle_{\rm s}$ and main domain width $\langle w\rangle_{\rm m}$ of the magnetic images, and average grain size $\langle d\rangle$ of the Sm–Co specimens.

Specimens	A	B	C	D
$\langle w\rangle_{\rm s}/\mu$m	0.9	1.5	1.6	0.5
$\langle w\rangle_{\rm m}/\mu$m	1.8	10.0	3.5	1.1
$\langle d\rangle/\mu$m	10	>40	>40	>40

2:17-type magnet.[10] It is noted that the single domain critical size of the 2:17 cell of high coercivity Sm–Co magnet is about 700 nm,[18] which is much larger than the cell size (about 100–200 nm). Therefore, the domain structures of specimen D are actually an aggregation of many single domains, or so-called coupling interaction domains,[10] which occurs usually in the various nanocomposite magnets.[19−21]

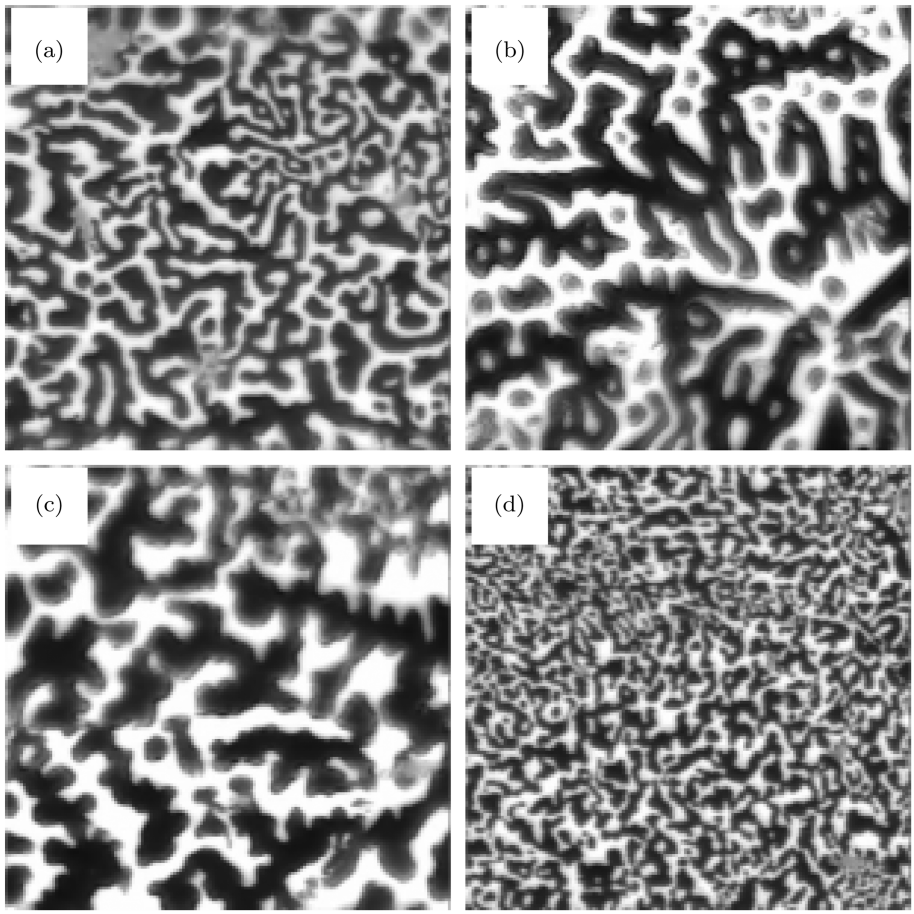


Fig.3. Typical magnetic force microscopy images of the four specimens with the normal c-axis perpendicular to the imaging plane. Scan area is $40\,\mu\text{m}\times 40\,\mu\text{m}$ for the images. Lift-height of the tips is 30 nm.

Moreover, for the specimens A–D with the c-axis parallel to the imaging plane as shown in Fig.4, their magnetic domains have also been revealed by MFM. In this case, the magnetic domain configurations of the four specimens are typically plate-like domains, which greatly differ from those shown in Fig.3 in domain patterns. Actually, the magnetic domains shown in Fig.4 are the interior domains of the corresponding specimens studied in Fig.3. Furthermore, it is obvious that the big difference in average domain width between the plate-like domains exists. In Fig.4, the values of average main domain width ($\langle w\rangle_{\rm m}$) of the specimens A–D are measured to be about 1.8, 10.0, 3.5 and 1.1 μm, respectively, and listed in Table 2. Comparing $\langle w\rangle_{\rm m}$ with $\langle w\rangle_{\rm s}$, it is found that the $\langle w\rangle_{\rm m}$ is two or more times larger than $\langle w\rangle_{\rm s}$ for the same group of specimens (see Table 2). The reason is that in Fig.4 the magnetostatic energy of the surface layer of the specimens is much smaller because the c-axis is parallel to the imaging plane, resulting in a larger domain width. In Fig.3, however, the c-axis of the measured specimens is perpendicular to the imaging plane and the narrow domain width is needed for reducing the magnetostatic energy of the surface layer. Observing Fig.4, it is impressive that among these domain widths the domain width of the specimen B, $\langle w\rangle_{\rm m}^{\rm B}$, is the largest (about 10 μm), which is about 6.7 times the surface domain width $\langle w\rangle_{\rm s}^{\rm B}$ of specimen B, indicating further that the corrugation and spike domain (Fig.3(b)) is the result of the branching of domains from interior to surface along the c-axis.

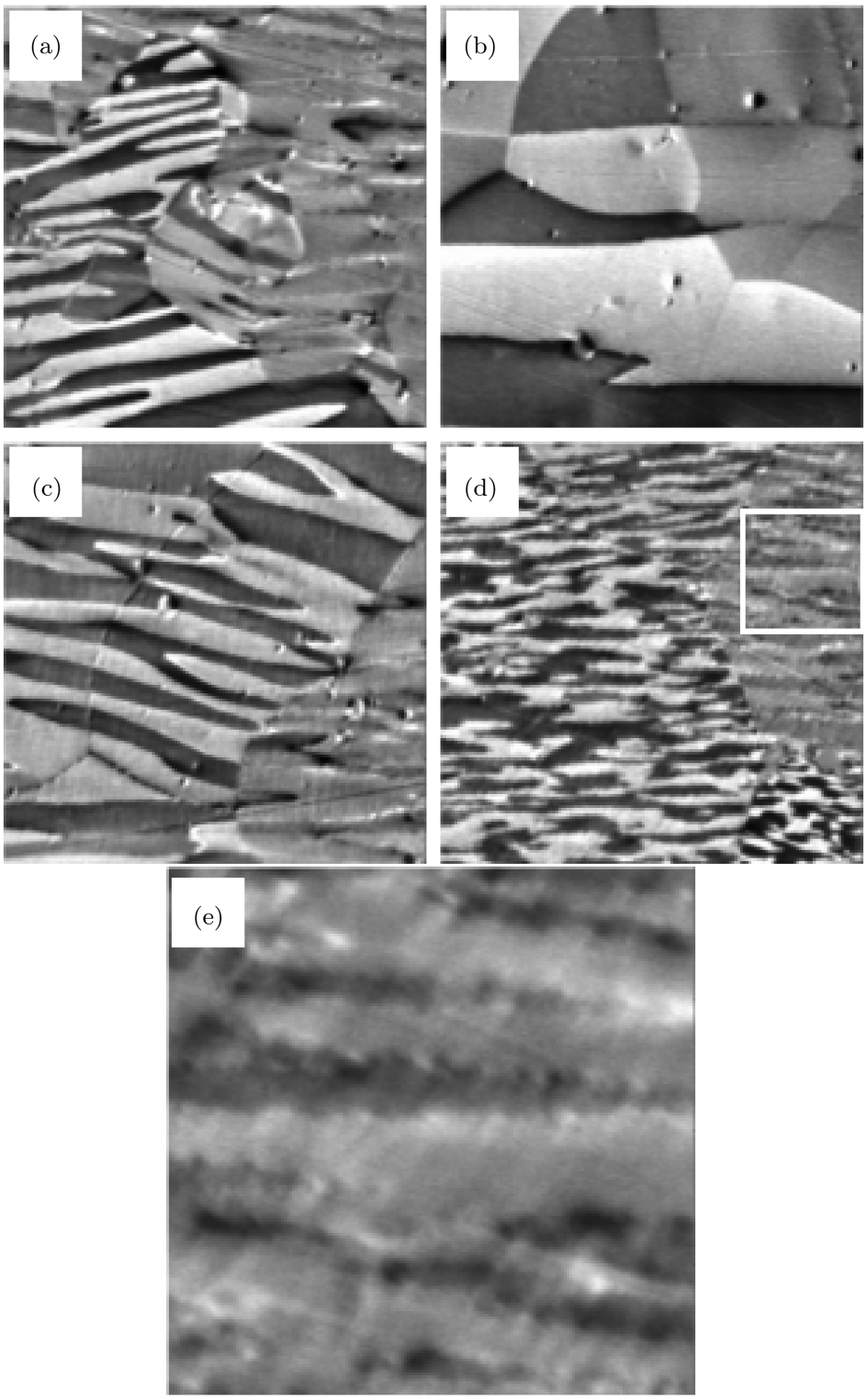


Fig.4. Typical magnetic force microscopy images of the four kinds of specimens with the *c*-axis parallel to the imaging plane. The region marked by a square in (d) is magnified into (e). Scan area is $40\,\mu$m$\times 40\,\mu$m for (a)–(d) and $10\,\mu$m$\times 10\,\mu$m for (e). Lift-height of the tips is 30 nm.

As shown in Fig.4, the different deviations of the plate-like domain orientation from the aligning direction (along the bottom side of the images), and the difference in darkness and whiteness between different crystals all indicate that the easy axes (c-axes) of the grains are distributed on a cone with respect to the aligning direction. In fact, the region with the same deviations of the plate-like domain orientation belongs to a grain due to the same directions of easy magnetization. Therefore, the grain size and the shape of the specimens can be recognized from the magnetic domain images. From the images similar to Figs.4(a)–4(d), the average grain size $\langle d \rangle$ of the specimen A is measured statistically to be about $10\,\mu$m, and the others are more than $40\,\mu$m, implying that the grains of the specimens apparently grow up after the solid solution has been treated at 1180°C for a relatively long time.

An area marked by a square in Fig.4(d) has been selected and scanned again. And a typical $10\,\mu\text{m}\times 10\,\mu$m magnetic image captured by MFM is shown in Fig.4(e). Obviously, the domain walls are formed in a zigzag shape, which has been detected early by using the high resolution Lorentz transmission electron microscopy (TEM).[8] However, it should be pointed out that the domain observation by TEM has only limited the relevance concerning the domain structures of bulk materials and the change of those structures in a magnetization process because domain structures are very sensitive to the sample thickness.[10,17] Therefore the domains in samples thinned for TEM investigation can be very different from those in the bulk samples. In our studies, the zigzag-shaped domain walls have also been revealed by MFM on the surface of bulk specimens with the normal c-axis parallel to the imaging plane. It has been accepted that the coercivity mechanism of the SmCo 2:17-type magnet at room temperature is the effect of domain wall pinning. The magnetic domain structures show that the wavy domain walls follow cell boundaries. It is presumed that these wavy domain walls act as the pinning centres during the magnetization reversal, resulting in a high intrinsic coercivity. Reasonably, the low values of intrinsic coercivity ($< 100\,$kA/m) of specimens A-C are ascribed to the large grain size and the weak pinning centre.

According to the obtained magnetic images (Figs.3 and 4) and the precipitation-hardened process of high temperature SmCo 2:17-type magnets, the schematic of magnetic microstructures from interior to surface for the specimens A–D are built and illustrated in Figs.5(a)–5(d), respectively, to show the evolution of magnetic domains. We believe that the considerable change of magnetic domains (Figs.3 and 4) of the specimens after quenched through different steps can be ascribed to the variation of main magnetic phase from 1:7 to 2:17 (verified by XRD results shown in Fig.1) and crystal size during the complex heat treatments (see Figs.4(a)–4(d)). As is well known, for high performance Sm–Co magnets, the variation of phase constituents and the corresponding intrinsic properties and the grain size as well are pronounced during the complex heat treatments. As mentioned above, the grain size of the specimen B is larger than that of specimen A. Therefore, for specimen B, the occurrence of corrugation and reverse spike domains near the surface results in a reduction of the magnetostatic energy at the cost of a larger total Bloch wall area,[22] as shown in Fig.5(b). Moreover, the development of cellular precipitation structure of high coercivity Sm–Co magnets is controlled by the growth of grain and the chemical redistribution process. The cellular precipitation structure is formed during the isothermal aging procedure, whereas the chemical redistribution of the transition metals during the slow-cooling procedure increases the coercivity of the final magnet. For specimen C as shown in Fig.5(c), spike domains are not needed on the balance between domain wall energy and demagnetization energy due to the formation of cellular structure from the phase separation of 1:7-type phase and the subsequent weakening of magnetic anisotropy of the obtained 2:17 main phase. However, for specimen D as shown in Fig.5(d), the fine scale domains form due to the further diffusion of copper from the interior of the 2:17 cells into the 1:5 boundary phase during the slow cooling ramp. This distribution of elements changes the intrinsic magnetic properties of the 1:5 phase, and then increases the difference in domain wall energy between the interior and the boundary of the cells.[14,15] Therefore, the significant difference in magnetic domain between specimens C and D (see Figs.3(c), 3(d), 4(c), and 4(d)) can be attributed to large fluctuations in the intrinsic properties of the 1:5 cell boundaries though they both exhibit cellular structures. Considering the evolution of magnetic domains and magnetic properties of the four specimens, it is reasonably deduced that the fine scale domain (Figs.3(d) and 4(d)) is a characteristic feature of SmCo 2:17-type sintered magnets with peculiar cellular nanostructures.

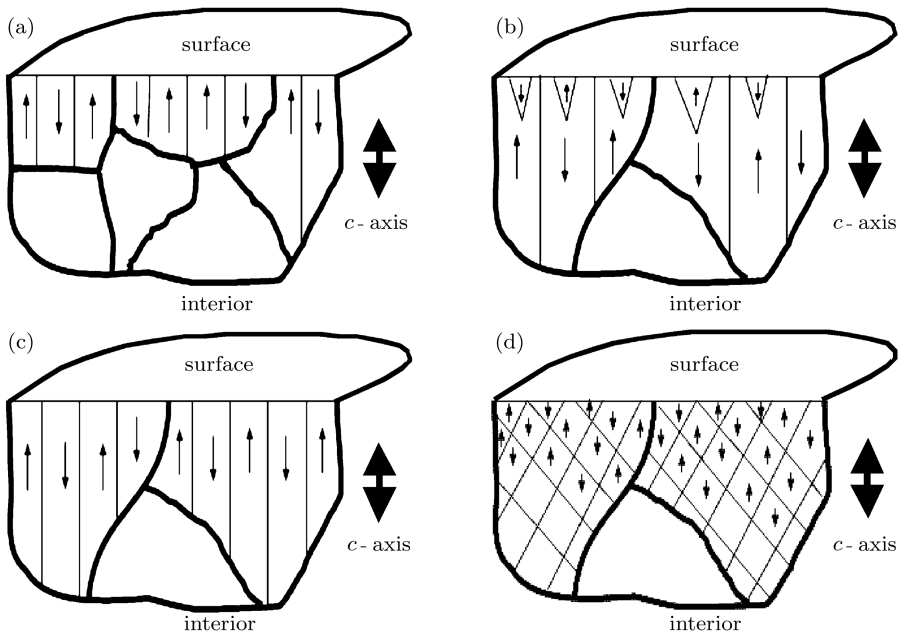


Fig.5. Schematic of magnetic microstructures from interior to surface for the specimens A (a), B (b), C (c) and D (d).

4. Conclusions

The crystal structures and magnetic properties of SmCo 2:17-type sintered magnets after quenching through complex processing steps (such as sintering, solid solution, isothermal and slow cooling) have been examined. Furthermore, magnetic domain structures of these SmCo 2:17-type magnets have been investigated by using magnetic force microscopy. The large difference in magnetic microstructure among the four specimens originates from the variation of phase structures (or the domain wall energy of the main phases) and the crystalline microstructures during heat treatments. The fine scale domain is a characteristic feature of SmCo 2:17-type sintered magnets with peculiar cellular nanostructures.

References

[1] Strnat K J 1988 *Ferromagnetic Materials* **4** (Amsterdam: North-Holland) pp131-209
[2] Chen C H, Walmer M S, Walmer M H, Liu S, Kuhl E and Simon G 1998 *J. Appl. Phys.* **83** 6706
[3] Hadjipanayis G C, Tang W, Zhang Y, Chui S T, Liu J F, Chen C and Kronmüller H 2000 *IEEE Trans. Magn.* **36** 3382
[4] Fidler J 1982 *J. Magn. Magn. Mater.* **30** 58
[5] Livingston J D and Martin D L 1977 *J. App1. Phys.* **48** 1350
[6] Yan A, Gutfleisch O, Handstein A, Gemming T and Müller K H 2000 *J. Appl. Phys.* **93** 7975
[7] Zhang Y and Hadjipanayis G C 2004 *IEEE Trans. Magn.* **40** 2925
[8] Zhang Y, Corte-Real M, Hadjipanayis G C, Liu J, Walmer M S and Krishnan K M 2000 *J. Appl. Phys.* **87** 6722
[9] Xia A L, Fang Y K, Guo Z H, Li W and Han B S 2006 *Chin. Phys. Lett.* **23** 1289
[10] Gutfleisch O, Müller K H, Khlopkov K, Wolf M, Yan A, Schäfer R, Gemming T and Schultz L 2006 *Acta Mater.* **54** 997
[11] Al-Khafaji M A, Marashi S P H, Rainforth W M, Gibbs M R J, Davies H A, Bishop J E L and Heydon G 1998 *J. Magn. Magn. Mater.* **190** 48
[12] Szmaja W 2006 *J. Magn. Magn. Mater.* **301** 546
Szmaja W 2007 *J. Magn. Magn. Mater.* **311** 469
[13] Xia A L, Guo Z H, Li W and Han B S 2006 *J. Rare Earth* **24** 214
[14] Yan A, Gutfleisch O, Gemming T and Müller K H 2003 *Appl. Phys. Lett.* **83** 2208
[15] Goll D, Kronmüller H and Stadelmaier H H 2004 *J. Appl. Phys.* **96** 6534
[16] Bodenberger R and Hubert A 1977 *Phys. Status Solidi* A **K7** 44
[17] Hubert A and Schäfer R 1998 *Magnetic Domains* (Berlin: Springer)
[18] Zhou S Z and Dong Q F 2004 *High Performance Nd-FeB Permanent Magnets* (Beijing: Metallurgical Industry Press) p228
[19] Fang Y K, Chang C W, Chang W C, Chen Q and Han B S 2005 *Chin. Phys. Lett.* **22** 1776
[20] Xia A L, Ge H L, Chang C W, Chang W C and Han B S 2006 *J. Magn. Magn. Mater.* **305** 336
[21] Chang C W, Chang H W, Chiu C H, Chang W C, Fang Y K and Han B S 2006 *J. Appl. Phys.* **99** 1
[22] Goodenough J B 1956 *Phys. Rev.* **102** 356